# Mechanistic basis of bell-shaped dependence of inositol 1,4,5-trisphosphate receptor gating on cytosolic calcium

Tadashi Shinohara[a,1], Takayuki Michikawa[a,b,1,2,3], Masahiro Enomoto[a,4], Jun-Ichi Goto[a,5], Miwako Iwai[c], Toru Matsu-ura[a,6], Haruka Yamazaki[a], Akitoshi Miyamoto[a,d], Akio Suzuki[a,7], and Katsuhiko Mikoshiba[a,b,2]

[a]Laboratory for Developmental Neurobiology, RIKEN Brain Science Institute, Wako, Saitama 351-0198, Japan; [b]Calcium Oscillation Project, International Cooperative Research Project and Solution-Oriented Research for Science and Technology, Japan Science and Technology Agency, Kawaguchi, Saitama 332-0012, Japan; and [c]Division of Molecular Pathology, Department of Cancer Biology, and [d]Division of Neuronal Network, Department of Basic Medical Sciences, Institute of Medical Science, University of Tokyo, Minato-ku, Tokyo 108-8639, Japan

Edited by Richard W. Aldrich, University of Texas, Austin, TX, and approved August 9, 2011 (received for review January 30, 2011)

**The inositol 1,4,5-trisphosphate ($IP_3$) receptor ($IP_3R$) is an intracellular $Ca^{2+}$ release channel, and its opening is controlled by $IP_3$ and $Ca^{2+}$. A single $IP_3$ binding site and multiple $Ca^{2+}$ binding sites exist on single subunits, but the precise nature of the interplay between these two ligands in regulating biphasic dependence of channel activity on cytosolic $Ca^{2+}$ is unknown. In this study, we visualized conformational changes in $IP_3R$ evoked by various concentrations of ligands by using the FRET between two fluorescent proteins fused to the N terminus of individual subunits. $IP_3$ and $Ca^{2+}$ have opposite effects on the FRET signal change, but the combined effect of these ligands is not a simple summative response. The bell-shaped $Ca^{2+}$ dependence of FRET efficiency was observed after the subtraction of the component corresponding to the FRET change evoked by $Ca^{2+}$ alone from the FRET changes evoked by both ligands together. A mutant $IP_3R$ containing a single amino acid substitution at K508, which is critical for $IP_3$ binding, did not exhibit this bell-shaped $Ca^{2+}$ dependence of the subtracted FRET efficiency. Mutation at E2100, which is known as a $Ca^{2+}$ sensor, resulted in ~10-fold reduction in the $Ca^{2+}$ dependence of the subtracted signal. These results suggest that the subtracted FRET signal reflects $IP_3R$ activity. We propose a five-state model, which implements a dual-ligand competition response without complex allosteric regulation of $Ca^{2+}$ binding affinity, as the mechanism underlying the $IP_3$-dependent regulation of the bell-shaped relationship between the $IP_3R$ activity and cytosolic $Ca^{2+}$.**

calcium signal | channel gating | ion channel

The inositol 1,4,5-trisphosphate ($IP_3$) receptor ($IP_3R$) is a dual-ligand–gated $Ca^{2+}$ release channel whose opening is controlled by $IP_3$ and $Ca^{2+}$ (1) and which plays a crucial role in the generation of $Ca^{2+}$ signals that control numerous cellular processes (2). Individual $IP_3R$ subunits possess a single $IP_3$ binding site (3) and multiple $Ca^{2+}$ binding sites (4, 5), and tetrameric complexes of these subunits form functional $IP_3$-gated $Ca^{2+}$ release channels (6). Cytoplasmic $Ca^{2+}$ regulates $IP_3R$ in a biphasic manner: $Ca^{2+}$ release is potentiated at low $Ca^{2+}$ concentrations but inhibited at higher $Ca^{2+}$ concentrations (7, 8). The stimulatory effect suggests that the channels display the process of $Ca^{2+}$-induced $Ca^{2+}$ release, which underlies $Ca^{2+}$ spike generation and wave propagation. In other words, the bell-shaped dependence on cytosolic $Ca^{2+}$ is the fundamental property of $IP_3R$ for the generation of $Ca^{2+}$ excitability (9).

$IP_3$ monotonically activates the $IP_3R$ channels at constant $Ca^{2+}$ concentrations (10), but $IP_3$ dynamically changes the $Ca^{2+}$ sensitivity of the channel (11, 12). At subsaturating concentrations of $IP_3$, the optimal $Ca^{2+}$ concentration for $IP_3R$ modulation becomes lower, whereas at very high concentrations of $IP_3$, channel activity persists at supramicromolar $Ca^{2+}$ concentrations (11, 12). This mechanism of dual-ligand regulation of the $IP_3R$ channel has attracted considerable interest, but the molecular dynamics underpinning this mechanism of $IP_3R$ channel gating is still controversial. Marchant and Taylor (13) have proposed that $IP_3$ binding evokes a rapid conformational change that exposes a high-affinity $Ca^{2+}$ binding site, to which $Ca^{2+}$ must bind before the channel can open. This model suggests that $Ca^{2+}$, but not $IP_3$, directly activates the $IP_3R$ channel. Foskett and colleagues (12) have proposed that $Ca^{2+}$ is the true agonist of $IP_3R$, whereas $IP_3$ acts as a regulatory factor that simply reduces the sensitivity of the receptor to the inhibition caused by high concentrations of $Ca^{2+}$. Foskett and colleagues (14) have also proposed a triumvirate of $Ca^{2+}$ binding sites that are involved in channel gating: $IP_3$-independent $Ca^{2+}$ binding sites responsible for channel activation, $IP_3$-independent $Ca^{2+}$ binding sites responsible for channel inactivation, and $IP_3$-dependent $Ca^{2+}$ binding sites that have opposite functions (activation or inhibition) depending on $IP_3$ binding. Evidence that substitution of a glutamate residue (E2100) in type 1 $IP_3R$ ($IP_3R1$) impairs (by 10-fold) $Ca^{2+}$ sensitivity for both $Ca^{2+}$-dependent activation and inactivation of $IP_3R1$ highlights a potential role of this residue in sensing $Ca^{2+}$ (15, 16). However, whether E2100 is involved in the $IP_3$-induced high-affinity $Ca^{2+}$ binding site (13) or in one of three $Ca^{2+}$ binding sites (14) is not known. No other $Ca^{2+}$ binding sites involved in the regulation of $IP_3R$ channel activity have been identified. Conversely, a further model has been proposed in which $IP_3$ is the functional ligand, inducing conformational changes in the N-terminal $IP_3$ binding domain that are mechanically transmitted to the opening of the pore through an attachment to the linker region between the fourth and fifth transmembrane regions (17).

Observation of the conformational changes evoked by $IP_3$ and/or $Ca^{2+}$ should facilitate understanding of the mechanism responsible for ligand regulation of $IP_3R$ channel activity. The N-terminal $IP_3$ binding domain is critical for functional coupling between $IP_3$ binding and channel opening (17–20), and thus the relative position of the N terminus may contain the information

Author contributions: T. Michikawa designed research; T.S., T. Michikawa, M.E., J.-I.G., M.I., T. Matsu-ura, H.Y., A.M., and A.S. performed research; T.S. and T. Michikawa analyzed data; and T.S., T. Michikawa, and K.M. wrote the paper.

The authors declare no conflict of interest.

This article is a PNAS Direct Submission.

[1]T.S. and T. Michikawa contributed equally to this work.

[2]To whom correspondence may be addressed E-mail: t-michikawa@brain.riken.jp or mikosiba@brain.riken.jp.

[3]Present address: Laboratory for Molecular Neurogenesis, RIKEN Brain Science Institute, Wako, Saitama 351-0198, Japan.

[4]Present address: Division of Signaling Biology, Ontario Cancer Institute and Department of Medical Biophysics, University of Toronto, Toronto, ON, Canada M5G 1L7.

[5]Present address: Department of Physiology, Yamagata University School of Medicine, Yamagata 990-9585, Japan.

[6]Present address: Department of Pathology and Laboratory of Medicine, University of Cincinnati, Cincinnati, OH 45267-0529.

[7]Present address: Laboratory for Synaptic Function, RIKEN Brain Science Institute, Wako, Saitama 351-0198, Japan.

This article contains supporting information online at www.pnas.org/lookup/suppl/doi:10.1073/pnas.1101677108/-/DCSupplemental.

that regulates the conductance of the $IP_3R$ channel. In this study, we detected both $IP_3$ binding- and $Ca^{2+}$ binding-induced conformational changes in the $IP_3R$ channel by measuring FRET between N-terminally fused fluorescent proteins on individual $IP_3R$ subunits. We found that the effects of these two ligands on the molecular conformation of the channel are different and that the combined effect is not a simple summative response. This approach offers unique insight into the mechanism of dual-ligand regulation of channel activation and inactivation of $IP_3R$.

## Results

**Fluorescent Protein–$IP_3R$ Fusion Proteins.** To monitor the ligand-induced conformational changes in mouse $IP_3R1$, enhanced cyan fluorescent protein (ECFP) or an improved yellow fluorescent protein, Venus, was fused to the N terminus of $IP_3R1$ (cR and vR, respectively) (Fig. 1*A*). Stable cell lines expressing cR or vR were established from the intrinsic $IP_3R$-deficient DT40 cells (21). Fig. 1*B* shows the Western blot analysis of the membrane fractions prepared from established cells by using anti-$IP_3R1$ monoclonal antibody 18A10 (22). The measurements of cytosolic $Ca^{2+}$ concentration ($[Ca^{2+}]$) changes evoked by B-cell receptor stimulation showed that both cR and vR retain $IP_3$-induced $Ca^{2+}$ release activity (Fig. S1). Cells expressing both cR and vR also exhibited $Ca^{2+}$ increases after B-cell receptor stimulation (Fig. S1). The apparent $IP_3$ binding dissociation constant of vR expressed in Sf9 cells was 21 nM ($n = 2$), which is consistent with that of wild-type (wt) $IP_3R1$ (28.6 nM) (23). Therefore, the N-terminal fusion did not interfere with the $IP_3$ binding. $IP_3$-gated $Ca^{2+}$ release channels are composed with homotetrameric and heterotetrameric complexes (6). Molecular mass of cR was measured by size-exclusion column chromatography (Fig. 1*C*). $IP_3R$ proteins were solubilized with 0.1% Nonidet P-40 from microsomal membranes prepared from HeLa cells and were applied to a size-exclusion column TSK-gel G4000SW. Exogenously expressed cR was eluted in similar fractions to those of endogenous $IP_3R1$ and exogenous wt $IP_3R1$ (Fig. 1*C*), which was coimmunoprecipitated with cR (Fig. S2). These results indicate that fluorescent protein did not interfere with the tetrameric formation of $IP_3R1$. Fig. 1*D* shows the subcellular distribution of cR and vR expressed in the same HeLa cells. ECFP and Venus signals were almost overlapped, suggesting that both cR and vR are similarly distributed on the endoplasmic reticulum (ER) in HeLa cells.

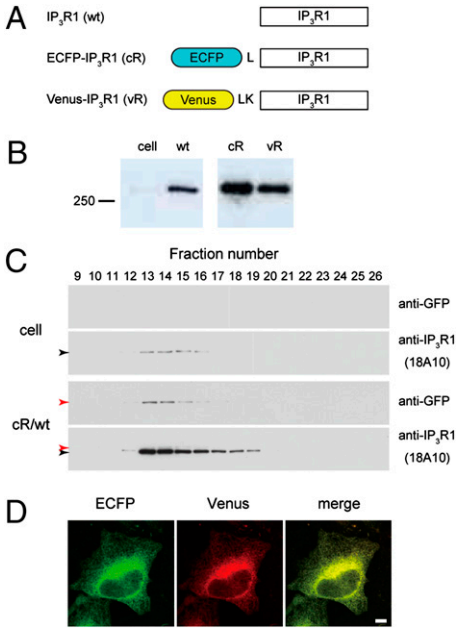


**Fig. 1.** Fluorescent protein–$IP_3R1$ fusions. (*A*) ECFP or Venus was fused to the N terminus of $IP_3R1$ with linker sequences. (*B*) Western blot analysis of cR and vR. Membrane proteins (10 μg) prepared from intrinsic $IP_3R$-deficient DT40 cells (cell) and stable cell lines expressing wt, cR, or vR were applied. Recombinant $IP_3Rs$ were detected with the antibody 18A10. A molecular size marker is shown on the left in kDa. (*C*) Lysates prepared from non-transfected HeLa cells (cell) and cells transfected with wt and cR cDNAs (cR/wt) were subjected to size-exclusion chromatography. Fractions from 9 to 26 were analyzed by Western blot using an anti-GFP antibody and 18A10. Black and red arrowheads indicate the position of wt and cR, respectively. The results were representative of three independent experiments. (*D*) HeLa cells transfected with cR and vR cDNAs were excited at 440 nm, and fluorescent signals (460–510 nm for ECFP and 515–620 nm for Venus) were monitored by confocal microscopy. (Scale bar: 10 μm.)

Cytosolic $Ca^{2+}$ dependence of fluorescent protein-tagged $IP_3R1$ was measured by ER luminal $Ca^{2+}$ imaging (Fig. S3). As shown in Fig. S3*A*, the addition of 1 μM $IP_3$ rapidly reduced the amount of $Ca^{2+}$ in the ER lumen in permeabilized HeLa cells. The rate of decrease in luminal $Ca^{2+}$ monotonically depends on the concentration of cytosolic $Ca^{2+}$ within the range examined (Fig. S3*B*). When wt $IP_3R1$ was expressed in HeLa cells, the rate of decrease in luminal $Ca^{2+}$ was substantially modified, and this modification exhibited a bell-shaped dependence on cytosolic $Ca^{2+}$ with a peak at ~0.4 μM $Ca^{2+}$ (Fig. S3*C*). The expression of the E2100Q mutant did not increase the rate of luminal $Ca^{2+}$ decrease within the range examined (Fig. S3*D*), suggesting that the $Ca^{2+}$ dependence of wt $IP_3R1$ channel activity directly reflects the modification of the rate of luminal $Ca^{2+}$ decrease. We found that HeLa cells expressing vR exhibit a similar biphasic $Ca^{2+}$ dependence on the modification of the rate of luminal $Ca^{2+}$ decrease (Fig. S3*E*). These results indicate that N-terminally fluorescent protein-tagged $IP_3R1$ is functional on the ER membrane in permeabilized HeLa cells and that the N-terminal fusion does not alter the $Ca^{2+}$ dependence of $IP_3R1$ channel activity.

The diameter of a tetrameric $IP_3R$ is ~20 nm (24, 25). When both cR and vR exist within a single tetramer, FRET from ECFP to Venus may occur because the Förster distance—the distance at which FRET efficiency is 50%—of the pair of ECFP and Venus is ~5 nm. By acceptor (Venus) photobleaching (Fig. S4*A*), the ECFP fluorescence intensity was increased to 118.0 ± 8.8% in HeLa cells expressing both cR and vR ($n = 92$). In HeLa cells transiently expressing cR or vR, the amount of exogenous fluorescent $IP_3R1$ proteins was comparable with that of endogenous $IP_3R1$ (Fig. S4*B*). These results indicate that a substantial amount of tetrameric $IP_3R$ complexes contain cR and vR and that the intermolecular FRET between cR and vR occurs in HeLa cells.

**Measurements of FRET Efficiency at Various Ligand Conditions.** To measure $IP_3$-dependent conformational changes of $IP_3R1$, HeLa cells expressing both cR and vR were permeabilized with 60 μM β-escin after treatments with 10 μM phospholipase C inhibitor U73122 and 1 μM thapsigargin, and then internal solutions containing various concentrations of free $IP_3$ were applied. As shown in Fig. 2*A*, $IP_3$ slightly increased the Venus/ECFP emission ratio (FRET signal). In contrast, the physiological concentration of free $Ca^{2+}$ in cytosol significantly decreased the FRET signal (Fig. 2*B*). The maximal normalized FRET signal change ($\Delta R/R_0$) evoked by $IP_3$ and $Ca^{2+}$ was 6.4% and −26.7%, respectively, and the apparent $IP_3$ and $Ca^{2+}$ sensitivity was 39 ± 25 and 122 ± 19 nM, respectively (Fig. 2 *C* and *D*). In the presence of $Ca^{2+}$, the application of $IP_3$ decreased the apparent $Ca^{2+}$ sensitivity of the FRET signals in an $IP_3$ dose-dependent manner (Fig. 2*B*). The results of dual-ligand application are summarized in Fig. 2*E*. Because the permeabilization treatment prevented the formation of $IP_3R1$ clusters on the ER (26), but did not inhibit $IP_3$-induced $Ca^{2+}$ release (Fig. S3), we consider that these FRET signals reflect conformational changes accompanying the channel gating of $IP_3R$ subunits.

From the slight convexity of the surface of the 3D plot (Fig. 2*E*), we noticed that the residual signals after the subtraction of $Ca^{2+}$-induced FRET signal changes measured without $IP_3$ from those measured with $IP_3$ exhibit a bell-shaped $Ca^{2+}$ dependence with a peak within a physiological range of $Ca^{2+}$ (Fig. 3*A*). The peak level of the residual signal increased and the $Ca^{2+}$ con-

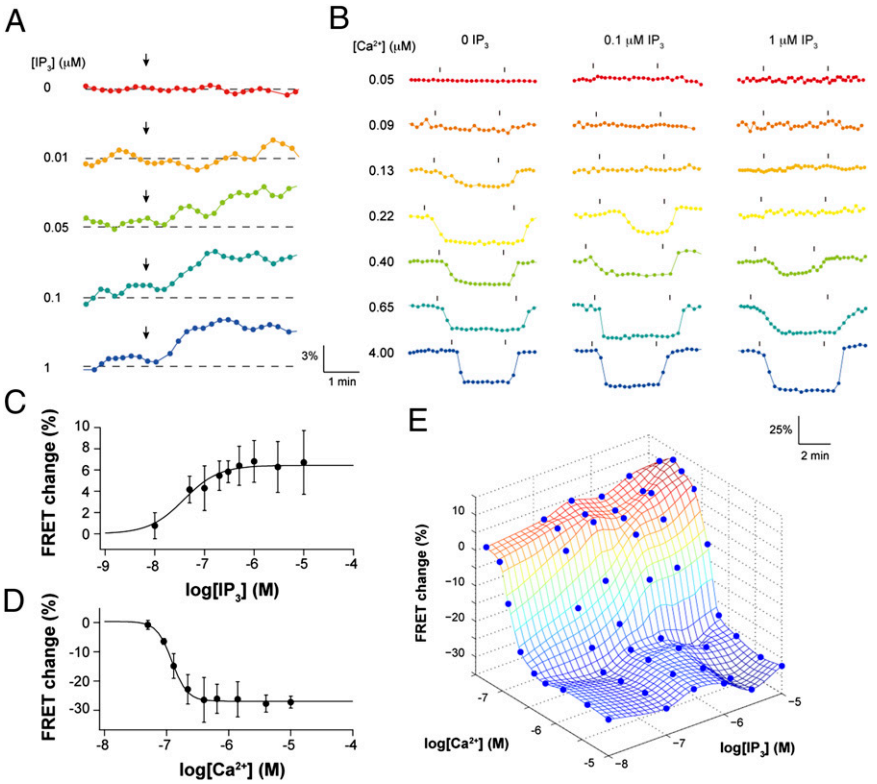


**Fig. 2.** $IP_3$- and/or $Ca^{2+}$-induced FRET signal changes. (*A*) Permeabilized HeLa cells expressing cR and vR were treated with the internal solution containing 5 mM EGTA and then with various concentrations of $IP_3$ after the time indicated by arrows. Normalized Venus/ECFP emission ratio changes ($\Delta R/R_0$) are shown. [$IP_3$] is shown on the left in μM. (*B*) Permeabilized HeLa cells expressing cR and vR were treated with the internal solution containing 5 mM EGTA and then with various concentrations of $Ca^{2+}$ and/or $IP_3$ during the period indicated by the vertical bars. Normalized Venus/ECFP emission ratio changes ($\Delta R/R_0$) are shown. Free [$Ca^{2+}$] is shown on the left in μM. (*C*) $IP_3$ dependence of FRET signal changes in the presence of 5 mM EGTA. Error bars correspond to SD. All values are relative to the FRET signal with zero $IP_3$ and 5 mM EGTA in *C*–*E*. (*D*) $Ca^{2+}$ dependence of FRET signal changes in the absence of $IP_3$. Error bars correspond to SD. (*E*) Steady-state FRET signals are plotted against [$Ca^{2+}$] and [$IP_3$]. The number of measurements is shown in Table S1.

centration at peak level moved to the right as $IP_3$ concentration ([$IP_3$]) increased (Fig. 3*B*), consistent with the $IP_3$ and $Ca^{2+}$ dependence of single-channel open probability of cerebellar $IP_3R$ recorded in planar lipid bilayers (7, 11). The residual signals after the subtraction of the $IP_3$-independent, $Ca^{2+}$-induced FRET signals were not detected in HeLa cells expressing $IP_3$ binding-deficient K508A mutants (Fig. 3*C*). These results indicate that the residual signals were evoked by $IP_3$ binding to $IP_3R1$. The substitution of E2100 induced a 10-fold lower shift in $Ca^{2+}$ sensitivity for both $Ca^{2+}$-dependent activation and inactivation of $IP_3R1$ when reconstituted into planar lipid bilayers (15, 16). The residual signals in the E2100Q mutant also showed a bell-shaped $Ca^{2+}$ dependence with ~10-fold lower $Ca^{2+}$ sensitivity compared with that of the wt channel (Fig. 3*D*). All these data strongly suggest that the positive FRET signal (i.e., increased FRET efficiency), which was uncovered by the subtraction of the $IP_3$-independent $Ca^{2+}$-induced FRET signal, directly reflects the conducting activity of $IP_3R1$.

**Construction of a Phenomenological $IP_3R$ Model.** In this study, we found that the activity of the $IP_3R1$ channel is proportional to the subtracted FRET signal, as follows:

$$activity \propto sFRET = FRET_{IP_3} - FRET_0, \qquad [1]$$

where *sFRET* is a subtracted FRET signal, $FRET_{IP_3}$ is the FRET signal in the presence of $IP_3$, and $FRET_0$ is the FRET signal in the absence of $IP_3$. When we use the Hill equation to fit the measured FRET signals with or without $IP_3$, we can express *sFRET* by the following equation:

$$sFRET = \left[B_0(\mathrm{IP_3}) + \{a - B_0(\mathrm{IP_3})\}\left\{1 + \left(\frac{K(\mathrm{IP_3})}{[\mathrm{Ca^{2+}}]}\right)^4\right\}^{-1}\right] - a\left\{1 + \left(\frac{b}{[\mathrm{Ca^{2+}}]}\right)^4\right\}^{-1}, \qquad [2]$$

where $a$ is the maximal FRET change of −26.7% (Fig. 4*A*), and $b$ is the apparent $Ca^{2+}$ affinity of the FRET signal in the absence of $IP_3$, which was estimated to be $1.33 \times 10^{-7}$ M (Fig. 4*D*; see below). The Hill coefficient is independent of [$IP_3$] and was estimated to be 4 (Fig. 4*B*). $B_0(IP_3)$ is the FRET signal in the absence of $Ca^{2+}$ and is a function of [$IP_3$] (Fig. 4*C*). $B_0(IP_3)$ can be expressed as

$$B_0(\mathrm{IP_3}) = c\left\{1 + \left(\frac{d}{[\mathrm{IP_3}]}\right)^{0.24}\right\}^{-1}, \qquad [3]$$

where $c$ is the maximal FRET change in the absence of $Ca^{2+}$ and was estimated to be 14.80% (Fig. 4*C*), $d$ is the apparent $IP_3$ affinity in the absence of $Ca^{2+}$ and was estimated to be $8.79 \times 10^{-7}$ M (Fig. 4*C*), and the Hill coefficient was estimated to be 0.24 (Fig. 4*C*). $K(IP_3)$ is the apparent $Ca^{2+}$ affinity of the FRET signal and is a function of [$IP_3$] (Fig. 4*D*). $K(IP_3)$ can be expressed as

$$K(\mathrm{IP_3}) = b + (e - b)\left(1 + \frac{f}{[\mathrm{IP_3}]}\right)^{-1}, \qquad [4]$$

where $e$ is the minimum apparent $Ca^{2+}$ affinity and was estimated to be $4.36 \times 10^{-7}$ M (Fig. 4*D*), and $f$ is the apparent $IP_3$ affinity and was estimated to be $4.70 \times 10^{-7}$ M (Fig. 4*D*). Fig. 4*E* shows the *sFRET* values calculated by Eqs. **2**–**4**. The calculated sFRET values provide a prediction of the activity of $IP_3R$ on the ER in permeabilized HeLa cells. When we adjust the parameters, Eqs. **2**–**4** can reproduce the phenomenon of very high [$IP_3$] compensating for the $Ca^{2+}$-dependent inactivation of $IP_3R$ (Fig. S5), which was shown previously by using cerebellar $IP_3R$ reconstituted into planar lipid bilayers (11).

## Discussion

In this study, we applied an optical technique to monitor conformational changes in $IP_3R$ channels and found that $IP_3$ and $Ca^{2+}$ have opposite effects on FRET signal changes. $IP_3$ binding

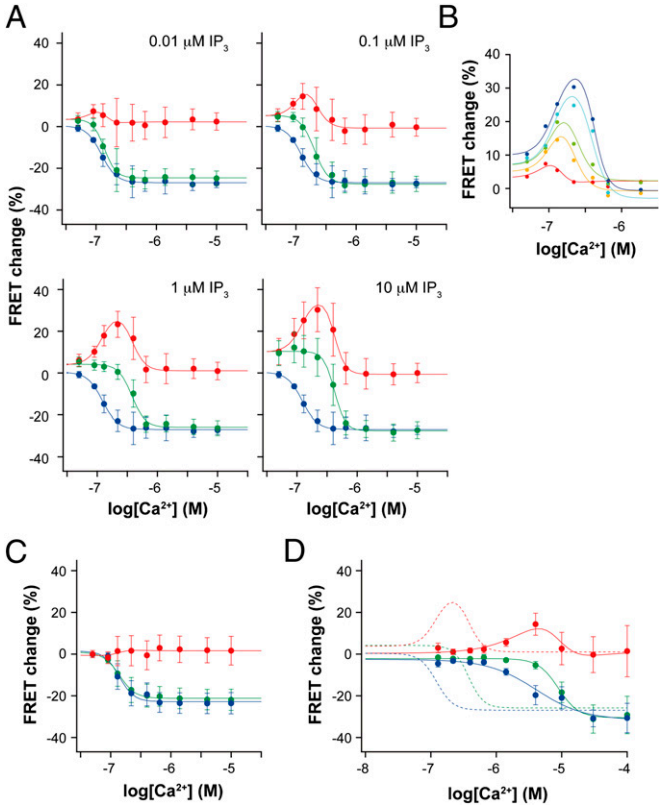


**Fig. 3.** Subtracted FRET signals. (*A*) FRET signals measured with (green) or without (blue) $IP_3$. The Hill equations fitted to the data are shown in colored smooth curves. Subtracted signals (green minus blue) are shown in red. The difference between two Hill equations is shown in red smooth curves. Error bars correspond to SD. (*B*) FRET signal changes in the presence of 0.01 (red), 0.1 (yellow), 0.3 (green), 3 (cyan), and 10 (blue) μM $IP_3$. (*C*) Results from cells expressing cR(K508A) and vR(K508A) at 1 μM $IP_3$. (*D*) Results from cells expressing cR(E2100Q) and vR(E2100Q) at 1 μM $IP_3$. Results from cells expressing nonmutated cR and vR at 1 μM $IP_3$ are shown in broken lines.

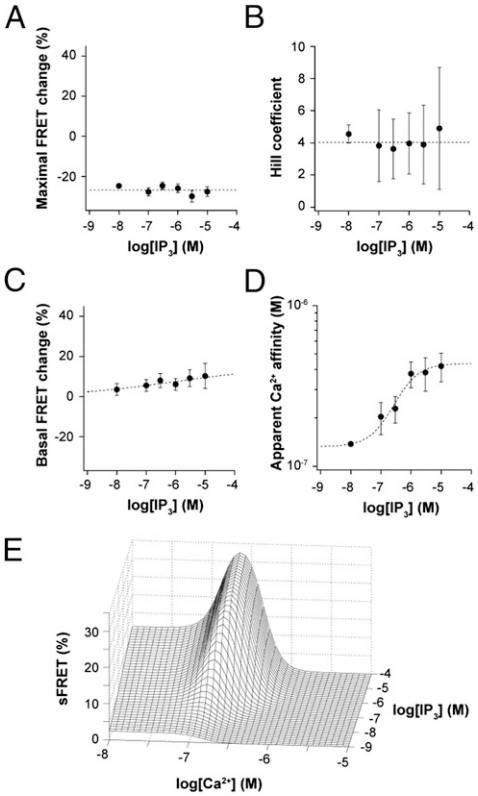


**Fig. 4.** An $IP_3R$ model based on the results of FRET imaging. (*A*) Estimated maximal FRET change. The broken line indicates a mean value of −26.7. (*B*) Estimated Hill coefficient. The broken line indicates a mean value of 4. (*C*) Estimated basal FRET change in the absence of $Ca^{2+}$. The data were fitted with Eq. **3** (broken line). (*D*) Estimated apparent $Ca^{2+}$ affinity. The data were fitted with Eq. **4** (broken line). (*E*) Plot of sFRET value calculated with Eqs. **2**–**4**.

increases FRET efficiency, indicating that differentially tagged N termini within a single tetrameric channel are brought closer together by changing the distance and/or angle between them. In contrast, $Ca^{2+}$ binding functions to decrease FRET efficiency, indicating that $Ca^{2+}$ binding induces a relaxation of tetrameric channel complexes. This $Ca^{2+}$-induced decrease in FRET efficiency is consistent with the results of single particle analysis showing that purified $IP_3R$ tetramers change their shape from a tight "square" form to a relaxed "windmill" form after $Ca^{2+}$ binding (25, 27). In this study, the magnitude of the FRET change evoked by $Ca^{2+}$ was larger than that evoked by $IP_3$ (Fig. 2 *C* and *D*), a feature consistent with the results of single particle analysis in which the effect of $IP_3$ addition on $IP_3R$ conformation was undetectably small (25, 27). In the presence of both $IP_3$ and $Ca^{2+}$, the conformational changes within the channel subunits are not a simple summation of those evoked by each ligand, because the dual-ligand–induced FRET signal changes were not as predicted for a summative response, as shown in Fig. 5*A*. The same concentration of $IP_3$ induced different degrees of FRET signal change depending on the concentration of $Ca^{2+}$ (Fig. 5*B*). A remarkable finding in this study was that, after subtraction of the FRET signal corresponding to the $Ca^{2+}$induced conformational change from the FRET signal corresponding to the gross conformational change evoked by $IP_3$ and $Ca^{2+}$ together, a bell-shaped dependence of FRET signal changes on cytosolic $Ca^{2+}$ was revealed (Fig. 3*A*). The other important finding is that the maximal FRET signal changes evoked by $Ca^{2+}$ were not affected by $IP_3$ concentration (Fig. 3*A*). If the maximal signal was increased by the addition of $IP_3$, the subtracted signal showed negative values at high $[Ca^{2+}]$ (Fig. 5*C*). The analyses of the mutant $IP_3R$ channels suggest that the subtracted FRET signal approximates the conducting activity of the channel (Fig. 3 *C* and *D*). These results demonstrate that the relative position of the N termini provides information concerning the gating activity of the tetrameric $IP_3R$ channel complex.

The findings in this study allowed us to construct a phenomenological model (Eqs. **2**–**4**) that quantitatively expresses the dependence of channel activity on $[IP_3]$ and $[Ca^{2+}]$. Formulation of the subtracted FRET signal showed that conformational changes accompanying channel gating can be divided into two components, which depend on $[Ca^{2+}]$ alone and both $[Ca^{2+}]$ and $[IP_3]$ (Eq. **2**). Although the sensitivity of the $IP_3R$ channel to $Ca^{2+}$-mediated activation is comparable in most measurements, the sensitivities to $Ca^{2+}$ inhibition are variable depending on the experimental approaches and/or conditions used to monitor single-channel currents. $IP_3Rs$ reconstituted into planar lipid bilayers are inhibited at $[Ca^{2+}]$ >1 μM (7), whereas $IP_3Rs$ in patch-clamped outer nuclear membranes are inhibited at $[Ca^{2+}]$ >10 μM (12). Purified $IP_3R$ reconstituted into planar lipid bilayers (28) and $IP_3R$ exposed to low $[Ca^{2+}]$ (<5 nM) for a few minutes before patch-clamp experiments (29) were not inhibited at high $[Ca^{2+}]$. These results indicate that the sensitivity to $Ca^{2+}$ inhibition is not an intrinsic property of the $IP_3R$ channel and is actively or passively regulated in individual cells. Therefore, parameters in Eq. **2** should be specific for the cell types examined. We demonstrated that our model, based on the results obtained from permeabilized HeLa cells, is applicable to single-channel data measured from $IP_3R$ reconstituted into planar lipid bilayers by tuning the Hill coefficient in

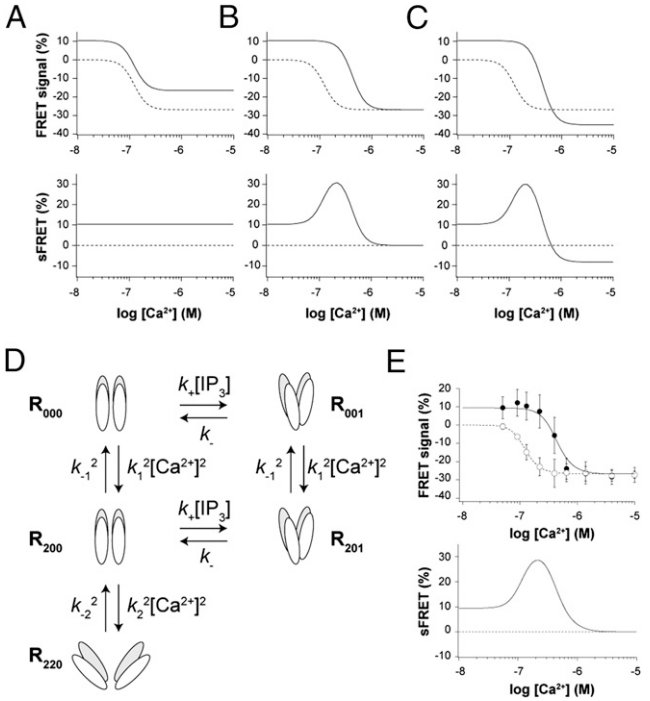


**Fig. 5.** Mechanism of dual-ligand regulation of $IP_3R$ channel gating. (*A*) Simulated linear summation. The FRET signal change in the absence of $IP_3$ (broken line) was calculated from parameters (basal FRET signal, maximal FRET change, apparent $Ca^{2+}$ sensitivity, and Hill coefficient) estimated from the data shown in Fig. 2*C*. For this signal, constant FRET signal (10%) was added (continuous line). Subtracted signal (continuous line–broken line) is shown in *Lower*. (*B*) Actual measurements. The FRET signal change in the presence of 10 μM $IP_3$ (continuous line) was calculated from the parameters estimated from the data shown in Fig. 2*C*. Subtracted signal (continuous line–broken line) is shown in *Lower*. (*C*) Variable maximal FRET changes. The maximal FRET signal was changed to −35% in the presence of 10 μM $IP_3$. All other parameters are the same as shown in *B*. Subtracted signal (continuous line–broken line) is shown in *Lower*. (*D*) A five-state model of $IP_3R$. $R_{000}$ is the unliganded state (FRET = 0%). $R_{200}$ is a state with two $Ca^{2+}$ binding sites occupied (FRET = 0%); $R_{220}$ is a state with four $Ca^{2+}$ binding sites occupied (FRET = −26.7%); $R_{001}$ is a state with a single $IP_3$ binding site occupied and all $Ca^{2+}$ binding sites unoccupied [FRET = $B_0(IP_3)$%]; and $R_{201}$ is a state with two $Ca^{2+}$ binding sites and an $IP_3$ binding site occupied [FRET = $B_0(IP_3)$%]. (*E*) Steady-state FRET signals calculated according to the model shown in *D* with the following parameters: $K_1 = k_{-1}/k_1 = 5.32 \times 10^{-7}$ (M); $K_2 = k_{-2}/k_2 = 5.32 \times 10^{-8}$ (M); $K = k_-/k_+ = 8.79 \times 10^{-7}$ (M); $k_1 = 2 \times 10^7$ ($M^{-1} \cdot s^{-1}$); and $k_+ = 4 \times 10^8$ ($M^{-1} \cdot s^{-1}$). Broken line: 0 $IP_3$; continuous line: 10 μM $IP_3$. Experimental data of FRET signals observed in the presence of zero $IP_3$ (open circles) and 10 μM $IP_3$ (filled circles) are shown. Data are mean ± SD. The subtracted signal (continuous line–broken line) is shown in *Lower*.

Eq. **2** and the parameters $c$, $e$, and $f$ (Fig. S5). The parameter $c$ is the maximal FRET change in the absence of $Ca^{2+}$ (Eq. **3**) and determines the channel activity at zero $Ca^{2+}$. The parameter $e$ is the minimum apparent $Ca^{2+}$ affinity and determines the lower limit of the sensitivity of $Ca^{2+}$ inhibition (Eq. **4**). The parameter $f$ is the apparent $IP_3$ affinity of the channel (Eq. **4**). The Hill coefficient in Eq. **2** reflects the degree of cooperativity of $Ca^{2+}$ binding. Identification of the factors that affect these parameters will facilitate understanding of the mechanism for generating diversity in the $Ca^{2+}$ sensitivity of the channel.

What can we extrapolate about the gating mechanism of the $IP_3R$ channel from the phenomenological model? The first term of Eq. **2** contains $K(IP_3)$ that corresponds to the apparent sensitivity of the FRET signal to $Ca^{2+}$ in the presence of $IP_3$. Because $K(IP_3)$ is a function of [$IP_3$] (Fig. 4*D*), it is possible to consider that $IP_3$ binding reduces the intrinsic affinity of $Ca^{2+}$ binding sites on the $IP_3R$ molecule for $Ca^{2+}$, as proposed previously (12). However, this relatively simple interpretation is unlikely because the $Ca^{2+}$-dependent activation of the channel occurs within a range of [$Ca^{2+}$] where the FRET signal is almost constant in the presence of $IP_3$. For example, the $IP_3R$ channel was markedly activated with 0.13 μM $Ca^{2+}$ in the presence of 1 μM $IP_3$ (7), even though 0.13 μM $Ca^{2+}$ is well below the $EC_{50}$ value of FRET change in the presence of 1 μM $IP_3$ (~0.38 μM; Fig. 3*A*). In addition, if the $IP_3$ binding selectively reduces the intrinsic $Ca^{2+}$ affinity of the binding sites responsible for $Ca^{2+}$-dependent inactivation without changing the affinity of the sites responsible for activation (12) or uncovers a hidden high-affinity $Ca^{2+}$ binding site for channel activation (13), changes in the Hill coefficient (Fig. 4*B*) and the maximal FRET signal (Fig. 4*A*) must be altered depending on [$IP_3$]. Therefore, we have formulated the alternate hypothesis of a dual-ligand regulation mechanism of $IP_3R$ channel gating.

Fig. 5*D* shows a state model that can reproduce the results of the FRET measurements from this study. In this model, four $Ca^{2+}$ ions and a single $IP_3$ molecule can bind to a single tetrameric channel. To reproduce the steep $Ca^{2+}$ dependence (Hill coefficient = 4) (Fig. 4*B*), two $Ca^{2+}$ ions are assumed to bind instantaneously. $IP_3$ binding increases the FRET signal according to Eq. **3**, irrespective of the binding of the first two $Ca^{2+}$ ions ($R_{001}$ and $R_{201}$; Fig. 5*D*). The binding of two $Ca^{2+}$ ions alone does not change the FRET signal ($R_{200}$, Fig. 5*D*), whereas the binding of the subsequent two $Ca^{2+}$ ions decreases the FRET signal to −26.7% ($R_{220}$ in Fig. 5*D*). This relatively simple model can reproduce the experimental results of the FRET measurements made in this study (Fig. 5*E*). Key features of our model are: (*i*) $IP_3$ binding does not change the intrinsic affinity of $IP_3R$ for $Ca^{2+}$; (*ii*) channels occupied with three and four $Ca^{2+}$ ions ($R_{210}$ and $R_{220}$, respectively) do not bind $IP_3$; (*iii*) $IP_3$ binding prevents the transition of the channel to the $R_{210}$ and $R_{220}$ states; (*iv*) $Ca^{2+}$ binding is a sequential process, and the binding of the first and second $Ca^{2+}$ ions is necessary for the binding of third and fourth $Ca^{2+}$ ions; and (*v*) the $Ca^{2+}$ binding affinity for the third and fourth $Ca^{2+}$ ions is higher than that of the first and second $Ca^{2+}$. The third feature is the cause of the apparent $IP_3$-induced reduction in the $Ca^{2+}$ sensitivity of the FRET signal change observed in the absence of any change in the intrinsic $Ca^{2+}$ binding affinity. The fifth feature is essential to reproduce the steep dependence of FRET changes on cytosolic $Ca^{2+}$, and it has not been reported previously. Our model is similar to the previous four-state model, which can reproduce frequency encoding by $Ca^{2+}$ oscillations and $Ca^{2+}$ wave propagation (30–32). Our model, however, can reproduce $IP_3$-dependent reduction of apparent $Ca^{2+}$ sensitivity of the channel, whereas the previous four-state models were constructed based on the steady-state bell-shaped $Ca^{2+}$ dependence of $IP_3R$ at a fixed concentration of $IP_3$ (2 μM). Remarkably, the number of states in our model is drastically smaller than that of previous models, which can reproduce $IP_3$-dependent reduction of $Ca^{2+}$ sensitivity, composed of 4,096 (11) or 3,750 (14) states.

We show here that the subtracted FRET signal reflects the activity of the $IP_3R$ channel. Which states are active in the model proposed? Foskett and colleagues (14) showed that $IP_3R$ exhibits $IP_3$-independent spontaneous opening in the absence of $Ca^{2+}$. These observations suggest that $R_{000}$ and $R_{001}$ possess an indistinguishable low open probability. We found that the subtracted FRET signal is a good approximation of the sum of the fraction of the state of $R_{201}$ and 0.075-fold of the fraction of the states of $R_{000}$ and $R_{001}$ (Fig. S6). These results indicate that (*i*) $R_{201}$ is the main conducting open state; (*ii*) $R_{000}$ and $R_{001}$ are open states with a low open probability; and (*iii*) $R_{220}$ is an inactivated state.

The state in which all of the ligand binding sites are occupied, $R_{221}$, is not present in the model shown in Fig. 5*D*. Therefore, high concentrations of $Ca^{2+}$ prevent $IP_3$ binding to the receptor in this model. This specific property is consistent with the previous experimental observations in which $IP_3$ binding to recombinant $IP_3R1$ expressed in Sf9 cells was examined under various concentrations of $Ca^{2+}$ (23, 33). Our model shows that $IP_3$ binding prevents binding of $Ca^{2+}$ to the inactivation sites and that, re-

ciprocally, $Ca^{2+}$ binding to the inactivation sites prevents $IP_3$ binding. Thus, there is no direct transition between the active $R_{201}$ state and the inactive $R_{220}$ state. We propose that this dual-ligand competition is the main mechanism underlying the $IP_3$-dependent regulation of the bell-shaped relationship between $IP_3R$ gating and cytosolic $Ca^{2+}$. This dual-ligand competition model reproduces the experimental results obtained by the FRET measurement without assuming a complex allosteric regulation of the affinity and function of $Ca^{2+}$ binding sites as proposed previously (14).

Single particle analysis has suggested that $Ca^{2+}$ binding induces structural transition from the tight square form to the relaxed windmill form (25, 27), but the relationship between the receptor structure and its function has not been examined. In this study, we found that the relaxed state ($R_{220}$, which may correspond to the windmill form) is an inactivated state, whereas the square form contains the active conducting state, $R_{201}$ (Fig. 5*D*). There are multiple $Ca^{2+}$ binding sites within a single $IP_3R$ subunit (4, 5). The $Ca^{2+}$ sensitivity of the FRET signal of the E2100Q mutant was reduced to 4.07 μM (from 122 nM in the wt channel) (Fig. 3*D*). The Hill coefficient was also reduced to 1.2, from 4 in the wt channel. However, the maximal FRET signal change of E2100Q was not altered (Fig. 3*D*). These results suggest that E2100 is involved in the $Ca^{2+}$ binding site responsible for the first two $Ca^{2+}$ ions that are involved in channel activation (Fig. 5*D*). Our analysis unveiled that there are two different types of $Ca^{2+}$ binding site within $IP_3R$: low-affinity sites responsible for channel activation and high-affinity sites responsible for channel inactivation. The four $Ca^{2+}$ binding sites proposed in this study are the minimal requirement. The measurement of the FRET signal used in this study will be useful for the identification of $Ca^{2+}$ binding sites involved in both the channel activation and inactivation and will further our understanding of the molecular basis of $IP_3R$ gating.

## Materials and Methods

HeLa cells expressing cR and vR were treated with 10 μM U73122 for 5 min and then with 1 μM thapsigargin for 5 min in balanced salt solution (BSS; 115 mM NaCl, 5.4 mM KCl, 1 mM $MgCl_2$, 10 mM glucose, and 20 mM Hepes–KOH, pH 7.4 at 37 °C) at 37 °C. After washing three times with BSS containing 5 mM EGTA, cells were permeabilized with 60 μM β-escin in the internal solution (19 mM NaCl, 125 mM KCl, 10 mM Hepes–KOH, pH 7.4 at 37 °C) containing 5 mM EGTA for 3–5 min. Permeabilized cells were gently washed with the internal solution containing 5 mM EGTA. Free $Ca^{2+}$ concentrations in the internal solutions were adjusted with $K_2$HEDTA and CaHEDTA at 37 °C according to the described method (28). Fluorescent signals were acquired with an IX-71 or IX-81 inverted microscope (Olympus), a cooled CCD camera ORCA-ER (Hamamatsu Photonics), and a 40× (n. a., 1.35) objective lens (Olympus), as described (34). A 425–445 nm excitation filter and a pair of 460- to 510-nm (ECFP) and 525- to 5,650-nm (Venus) emission filters were used. The images were captured at every 2–30 s with an exposure time of 100–150 ms. The emission ratio was calculated after subtraction of the background fluorescence. The Venus/ECFP emission ratio was defined as $R$, and $\Delta R$ was defined as $R - R_0$, where $R_0$ is the basal level. Cells showing the initial ratio of 1.50 ± 0.37 (from 0.90 to 3.54; $n$ = 3,295) were used for FRET measurements. The data acquisition was performed with TI Workbench and MetaMorph/MetaFluor software (Molecular Devices). Off-line analysis was performed with TI Workbench and Igor Pro software.

Other methods are provided in *SI Materials and Methods*.

**ACKNOWLEDGMENTS.** We thank Dr. A. Miyawaki (RIKEN Brain Science Institute) for the gift of the Venus cDNA and valuable discussion; K. Sawaguchi for technical assistance; and Drs. T. Inoue, H. Nakamura, M. Ikura, and M. W. Sherwood for fruitful discussion. This work was supported by grants from the RIKEN Special Postdoctoral Researchers Program (to M.E., T. Matsu-ura, and H.Y.) and by Ministry of Education, Culture, Sports, Science and Technology of Japan Grants 20700344 (to M.E.), 20370054 (to T. Michikawa), and 20220007 (to K.M.).

1. Finch EA, Turner TJ, Goldin SM (1991) Calcium as a coagonist of inositol 1,4,5-trisphosphate-induced calcium release. *Science* 252:443–446.
2. Berridge MJ (1993) Inositol trisphosphate and calcium signalling. *Nature* 361: 315–325.
3. Maeda N, Niinobe M, Mikoshiba K (1990) A cerebellar Purkinje cell marker $P_{400}$ protein is an inositol 1,4,5-trisphosphate ($InsP_3$) receptor protein. Purification and characterization of $InsP_3$ receptor complex. *EMBO J* 9:61–67.
4. Sienaert I, et al. (1996) Characterization of a cytosolic and a luminal $Ca^{2+}$ binding site in the type I inositol 1,4,5-trisphosphate receptor. *J Biol Chem* 271:27005–27012.
5. Sienaert I, et al. (1997) Molecular and functional evidence for multiple $Ca^{2+}$-binding domains in the type 1 inositol 1,4,5-trisphosphate receptor. *J Biol Chem* 272: 25899–25906.
6. Monkawa T, et al. (1995) Heterotetrameric complex formation of inositol 1,4,5-trisphosphate receptor subunits. *J Biol Chem* 270:14700–14704.
7. Bezprozvanny I, Watras J, Ehrlich BE (1991) Bell-shaped calcium-response curves of $Ins(1,4,5)P_3$- and calcium-gated channels from endoplasmic reticulum of cerebellum. *Nature* 351:751–754.
8. Iino M (1990) Biphasic $Ca^{2+}$ dependence of inositol 1,4,5-trisphosphate-induced Ca release in smooth muscle cells of the guinea pig taenia caeci. *J Gen Physiol* 95:1103–1122.
9. Keizer J, Li YX, Stojilković S, Rinzel J (1995) $InsP_3$-induced $Ca^{2+}$ excitability of the endoplasmic reticulum. *Mol Biol Cell* 6:945–951.
10. Watras J, Bezprozvanny I, Ehrlich BE (1991) Inositol 1,4,5-trisphosphate-gated channels in cerebellum: presence of multiple conductance states. *J Neurosci* 11:3239–3245.
11. Kaftan EJ, Ehrlich BE, Watras J (1997) Inositol 1,4,5-trisphosphate ($InsP_3$) and calcium interact to increase the dynamic range of $InsP_3$ receptor-dependent calcium signaling. *J Gen Physiol* 110:529–538.
12. Mak DO, McBride S, Foskett JK (1998) Inositol 1,4,5-trisphosphate activation of inositol trisphosphate receptor $Ca^{2+}$ channel by ligand tuning of $Ca^{2+}$ inhibition. *Proc Natl Acad Sci USA* 95:15821–15825.
13. Marchant JS, Taylor CW (1997) Cooperative activation of $IP_3$ receptors by sequential binding of $IP_3$ and $Ca^{2+}$ safeguards against spontaneous activity. *Curr Biol* 7:510–518.
14. Mak DO, McBride SM, Foskett JK (2003) Spontaneous channel activity of the inositol 1,4,5-trisphosphate ($InsP_3$) receptor ($InsP_3R$). Application of allosteric modeling to calcium and $InsP_3$ regulation of $InsP_3R$ single-channel gating. *J Gen Physiol* 122:583–603.
15. Miyakawa T, et al. (2001) $Ca^{(2+)}$-sensor region of $IP_{(3)}$ receptor controls intracellular $Ca^{(2+)}$ signaling. *EMBO J* 20:1674–1680.
16. Tu H, et al. (2003) Functional and biochemical analysis of the type 1 inositol (1,4,5)-trisphosphate receptor calcium sensor. *Biophys J* 85:290–299.
17. Schug ZT, Joseph SK (2006) The role of the S4-S5 linker and C-terminal tail in inositol 1,4,5-trisphosphate receptor function. *J Biol Chem* 281:24431–24440.
18. Chan J, et al. (2010) Structural studies of inositol 1,4,5-trisphosphate receptor: coupling ligand binding to channel gating. *J Biol Chem* 285:36092–36099.
19. Uchida K, Miyauchi H, Furuichi T, Michikawa T, Mikoshiba K (2003) Critical regions for activation gating of the inositol 1,4,5-trisphosphate receptor. *J Biol Chem* 278: 16551–16560.
20. Yamazaki H, Chan J, Ikura M, Michikawa T, Mikoshiba K (2010) Tyr-167/Trp-168 in type 1/3 inositol 1,4,5-trisphosphate receptor mediates functional coupling between ligand binding and channel opening. *J Biol Chem* 285:36081–36091.
21. Sugawara H, Kurosaki M, Takata M, Kurosaki T (1997) Genetic evidence for involvement of type 1, type 2 and type 3 inositol 1,4,5-trisphosphate receptors in signal transduction through the B-cell antigen receptor. *EMBO J* 16:3078–3088.
22. Maeda N, Niinobe M, Nakahira K, Mikoshiba K (1988) Purification and characterization of $P_{400}$ protein, a glycoprotein characteristic of Purkinje cell, from mouse cerebellum. *J Neurochem* 51:1724–1730.
23. Iwai M, et al. (2005) Molecular cloning of mouse type 2 and type 3 inositol 1,4,5-trisphosphate receptors and identification of a novel type 2 receptor splice variant. *J Biol Chem* 280:10305–10317.
24. Chadwick CC, Saito A, Fleischer S (1990) Isolation and characterization of the inositol trisphosphate receptor from smooth muscle. *Proc Natl Acad Sci USA* 87:2132–2136.
25. Hamada K, Miyata T, Mayanagi K, Hirota J, Mikoshiba K (2002) Two-state conformational changes in inositol 1,4,5-trisphosphate receptor regulated by calcium. *J Biol Chem* 277:21115–21118.
26. Tateishi Y, et al. (2005) Cluster formation of inositol 1,4,5-trisphosphate receptor requires its transition to open state. *J Biol Chem* 280:6816–6822.
27. Hamada K, Terauchi A, Mikoshiba K (2003) Three-dimensional rearrangements within inositol 1,4,5-trisphosphate receptor by calcium. *J Biol Chem* 278:52881–52889.
28. Michikawa T, et al. (1999) Calmodulin mediates calcium-dependent inactivation of the cerebellar type 1 inositol 1,4,5-trisphosphate receptor. *Neuron* 23:799–808.
29. Mak DO, McBride SM, Petrenko NB, Foskett JK (2003) Novel regulation of calcium inhibition of the inositol 1,4,5-trisphosphate receptor calcium-release channel. *J Gen Physiol* 122:569–581.
30. Bezprozvanny I (1994) Theoretical analysis of calcium wave propagation based on inositol (1,4,5)-trisphosphate ($InsP_3$) receptor functional properties. *Cell Calcium* 16: 151–166.
31. Bezprozvanny I, Ehrlich BE (1994) Inositol (1,4,5)-trisphosphate ($InsP_3$)-gated Ca channels from cerebellum: Conduction properties for divalent cations and regulation by intraluminal calcium. *J Gen Physiol* 104:821–856.
32. Othmer HG, Tang Y (1993) Oscillations and waves in a model of $InsP_3$-controlled calcium dynamics. *Experimental and Theoretical Advances in Biological Pattern Formation*, eds Othmer HG, Maini PK, Murray JD (Plenum, New York), pp 277–300.
33. Yoneshima H, Miyawaki A, Michikawa T, Furuichi T, Mikoshiba K (1997) $Ca^{2+}$ differentially regulates the ligand-affinity states of type 1 and type 3 inositol 1,4,5-trisphosphate receptors. *Biochem J* 322:591–596.
34. Matsu-ura T, et al. (2006) Cytosolic inositol 1,4,5-trisphosphate dynamics during intracellular calcium oscillations in living cells. *J Cell Biol* 173:755–765.